Advanced Technologies in Earth Sciences

Michael Weber
Ute Münch *Editors*

Tomography of the Earth's Crust: From Geophysical Sounding to Real-Time Monitoring

GEOTECHNOLOGIEN
Science Report No. 21

GEOTECHNOLOGIEN

Springer

Advanced Technologies in Earth Sciences

For further volumes:
http://www.springer.com/series/8384

Michael Weber · Ute Münch
Editors

Tomography of the Earth's Crust: From Geophysical Sounding to Real-Time Monitoring

GEOTECHNOLOGIEN Science
Report No. 21

Springer

Editors
Michael Weber
Department of Physics of the Earth
GFZ, German Research Centre for
Geosciences
Potsdam
Germany

Ute Münch
Coordination Office
GEOTECHNOLOGIEN
Potsdam
Germany

ISSN 2190-1635 ISSN 2190-1643 (electronic)
ISBN 978-3-319-04204-6 ISBN 978-3-319-04205-3 (eBook)
DOI 10.1007/978-3-319-04205- 3
Springer Cham Heidelberg New York Dordrecht London

Library of Congress Control Number: 2013958388

Printed on acid-free paper

Springer is part of Springer Science+Business Media (www.springer.com)

Foreword

Advanced Technologies in Earth Sciences is based in the German Geoscientific Research and Development Program "GEOTECHNOLOGIEN" funded by the Federal Ministry of Education and Research (BMBF) and the German Research Foundation (DFG).

This program comprises a nationwide network of transdisciplinary research projects and incorporates numerous universities, nonuniversity research institutions and companies. The books in this series deal with research results from different innovative geoscientific research areas, interlinking a broad spectrum of disciplines with a view to documenting System Earth as a whole, including its various subsystems and cycles. The research topics are predefined to meet scientific, sociopolitical, and economic demands for the future.

Ute Münch
Ludwig Stroink
Volker Mosbrugger
Gerold Wefer

Preface

The zone near the surface of our planet is the interface between geo-, bio-, hydro-, and atmosphere and the basis for our daily life. Water, natural resources (salt, ore, oil, and gas) and energy, for example heat, are exploited from this zone. Increasingly, waste and other material will be stored underground. We do not only use the surface for infrastructure but rather we increasingly expand construction to the subsurface for example relocating traffic to tunnels.

Suitable exploration and monitoring technologies are therefore of enormous importance to mitigate danger and damages in this economically and ecologically sensitive area. High resolution time-dependent images are necessary to derive crucial information about the subsurface. Thus, there is an urgent need for technologies and methods which enable high-resolution imaging of structures and processes in the subsoil on different spatial and time scales. The objective of this research topic was therefore the refinement of tomographic methods and their application to geological processes.

Despite methodical progress, especially in mathematical and numerical geophysics during the last few years, like the real-time data acquisition and evaluation in addition to computer-aided visualization programs, various methods are often still used independently due to economical reasons. However, the concerted combination and the enhancement of different methods allow new prospecting strategies.

The research work on the topic of "Tomography of the Earth's Crust: From Geophysical Sounding to Real-Time Monitoring" has focused on the development of cross-scale multiparameter methods and their technological application together with the development of innovative field techniques. Seismic wave field inversion theory, diffusion and potential methods were developed and optimized with respect to cost and benefit aspects.

This volume summarizes the scientific results of nine interdisciplinary joint projects funded by the German Federal Ministry of Education and Research in the framework of the Research and Development Program GEOTECHNOLOGIEN.

Highlights and innovations presented cover many length scales and involve targets ranging from applications in the laboratory, to ground water surveys of heterogeneous aquifer, geotechnical applications like tunnel excavation, coal mine and CO_2 monitoring and the imaging and monitoring of tectonic and societally relevant objects as active faults and volcanoes.

To study these objects, the authors use the full spectrum of geophysical methods (ultrasonics, seismic and seismology, electromagnetics, gravity, and airborne) in combination with new methods like seismic interferometry, diffuse wave field theory and full-wave-form inversion in 3D and partially also in 4D.

To make the results and implementations available to a broader community as well as to end-users, unique knowledge-based platforms were developed in terms of computer code, benchmark data, technical definitions, and recommendations via a web portal.

Ute Münch
Head of the GEOTECHNOLOGIEN coordination office

Michael Weber
Director of Department "Physics of the Earth"
German Research Centre for Geosciences, GFZ

Contents

Chapter 1
Broadband Electrical Impedance Tomography for Subsurface Characterization Using Improved Corrections of Electromagnetic Coupling and Spectral Regularization

Andreas Kemna, Johan A. Huisman, Egon Zimmermann, Roland Martin, Yulong Zhao, Andrea Treichel, Adrian Flores Orozco and Thomas Fechner

Abstract The low-frequency complex electrical conductivity in the mHz to kHz range has been shown to enable an improved textural, hydraulic, and biogeochemical characterization of the subsurface using electrical impedance spectroscopy (EIS) methods. Principally, these results can be transferred to the field using electrical impedance tomography (EIT). However, the required accuracy of 1 mrad in the phase measurements is difficult to achieve for a broad frequency bandwidth because of electromagnetic (EM) coupling effects at high frequencies and the lack of inversion schemes that consider the spectral nature of the complex electrical conductivity. Here, we overcome these deficiencies by (i) extending the standard spatial-smoothness constraint in EIT to the frequency dimension, thus enforcing smooth spectral signatures, and (ii) implementing an advanced EM coupling removal procedure using a newly formulated forward electrical model and calibration measurements. Both methodological advances are independently validated, and the improved imaging capability of the overall methodology with respect to spectral electrical properties is demonstrated using borehole EIT measurements in a heterogeneous aquifer. The developed procedures represent a significant step forward towards broadband EIT, allowing transferring the considerable diagnostic potential of EIS in the mHz to kHz

A. Kemna (✉) · R. Martin · A. Flores Orozco
Geodynamics/Geophysics, Steinmann Institute, University of Bonn, Meckenheimer Allee 176, 53115 Bonn, Germany
e-mail: kemna@geo.uni-bonn.de

J. A. Huisman · A. Treichel
Forschungszentrum Jülich GmbH, Institute for Bio- and Geosciences – Agrosphere (IBG 3), 52425 Jülich, Germany

E. Zimmermann · Y. Zhao
Forschungszentrum Jülich GmbH, Central Institute for Engineering, Electronics, and Analytics – Electronic systems (ZEA 2), 52425 Jülich, Germany

T. Fechner
Geotomographie GmbH, Am Tonnenberg 18, 56567 Neuwied, Germany

M. Weber and U. Münch (eds.), *Tomography of the Earth's Crust: From Geophysical Sounding to Real-Time Monitoring*, Advanced Technologies in Earth Sciences,
DOI: 10.1007/978-3-319-04205-3_1,

range to geophysical imaging applications at the field scale for improved subsurface characterization.

1.1 Introduction

Spectral induced polarization (SIP), also known as electrical impedance spectroscopy (EIS), is a geophysical method to measure the frequency-dependent complex electrical conductivity of soils, sediments, and rocks in the mHz to kHz range. In the absence of electronically conducting minerals, the real part of the complex electrical conductivity is a measure of ionic conduction in the water-filled pores and along water-mineral interfaces. The imaginary part of the complex conductivity is a measure of ionic polarization in response to an external electric field associated with electrically charged mineral surfaces and constrictions in the pore space (e.g., Leroy et al. 2008; Revil 2013). EIS can be implemented in a tomographic framework (e.g., Kemna et al. 2000), and is then commonly referred to as electrical impedance tomography (EIT).

In the last decades, EIS and EIT have been increasingly used in a wide range of applications, including lithological and textural characterization (e.g., Vanhala 1997; Slater and Lesmes 2002), direct estimation of hydraulic conductivity (e.g., Kemna et al. 2004; Binley et al. 2005; Revil and Florsch 2010), delineation of contaminant plumes (e.g., Kemna et al. 2004; Flores Orozco et al. 2012a), and monitoring of biogeochemical processes associated with contaminant remediation (e.g., Williams et al. 2009; Flores Orozco et al. 2013). The potential of EIS measurements for these applications has been clearly demonstrated in laboratory studies. It arises from the fact that the complex conductivity is directly affected by pore space geometry, pore fluid chemistry, and mineral surface properties. However, it is currently still difficult to fully capitalize on the recognized diagnostic capabilities of EIS measurements in EIT field applications (Kemna et al. 2012).

A first difficulty that currently limits the value of EIT measurements is that existing EIT inversion approaches treat all frequencies independently. This may lead to inconsistent imaging results that do not adequately capture the smooth and relatively weak frequency dependence of the complex electrical conductivity that has been reported in most studies dealing with the electrical properties of soils, sediments, and rocks.

A second reason why currently EIT is not able to deliver its full potential is related to the required high accuracy of 1 mrad in the phase measurements over a broad frequency range, extending from mHz to kHz. In recent years, considerable progress has been made with respect to understanding, quantifying, and correcting different error sources present in laboratory EIS and EIT measurements above 10 Hz (Zimmermann et al. 2008a, b). Despite this instrumental progress, it is still not possible to achieve such a high accuracy for a broad frequency bandwidth in EIT field applications. This is related to electromagnetic (EM) coupling effects that considerably affect EIT measurements at frequencies above ~10 Hz (e.g., Madden

and Cantwell 1967). This EM coupling is mainly caused by capacitive and inductive coupling between the electrical wires or between the wires and the soil and is thus inherent to field EIT measurements.

Within this context, the project '4D Spectral Electrical Impedance Tomography—a diagnostic imaging tool for the characterization of subsurface structures and processes (4DEIT)' was formulated. The main aims of this project were threefold. A first aim was to extend the standard spatial-smoothness constraint in EIT to the frequency dimension in order to obtain consistent imaging results across multiple frequencies. The developed approach was implemented in an existing EIT inversion code and validated using laboratory EIT measurements. A second aim was to develop correction procedures for inductive and capacitive coupling in EIT measurements made with multi-electrode chains. Controlled test measurements in a water-filled container were used for initial validation of the correction procedures and to determine the maximum expected accuracy that can be achieved using EIT field measurements of the complex electrical conductivity. A final aim was to evaluate these methodological advances using borehole EIT measurements made in the heterogeneous aquifer of the Krauthausen test site. In the following, we report on the main scientific findings of the 4DEIT project.

1.2 Inversion Methodology

1.2.1 EIT Inversion Approach

Electrical impedance tomography involves the inversion of a set of transfer impedances, Z, measured on an array of electrodes using a series of individual four-electrode configurations, into a distribution of complex resistivity, $\rho = |\rho| e^{j\phi}$ (with resistivity magnitude $|\rho|$, resistivity phase ϕ, and imaginary unit $j^2 = -1$), or complex electrical conductivity $\sigma = |\sigma| e^{-j\phi} = \sigma' + i\sigma''$ (with conductivity magnitude $|\sigma| = 1/|\rho|$, conductivity phase $-\phi$, real part of conductivity σ', and imaginary part of conductivity σ'').

We here build upon the finite-element based, smoothness-constraint inversion code by Kemna (2000), in which log-transformed impedances are used as data and log-transformed complex conductivities (of lumped finite-element cells) as parameters to account for the large range of resistance values in typical EIT data sets and of resistivity values for earth materials, respectively. For standard single-frequency, i.e., non-spectral, applications, the algorithm follows a standard Gauss-Newton procedure for non-linear inverse problems and iteratively minimizes an objective function, $\Psi(\mathbf{m})$, composed of the measures of data misfit and spatial model roughness, with both terms being balanced by a regularization parameter λ:

$$\Psi(\mathbf{m}) = \|\mathbf{W}\,[\mathbf{d} - \mathbf{f}(\mathbf{m})]\,\|^2 + \lambda\,\|\mathbf{R}\mathbf{m}\|^2\,, \tag{1.1}$$

where $\mathbf{d}$ is the data vector, $\mathbf{m}$ the model vector, $\mathbf{f}(\mathbf{m})$ the operator of the finite-element forward model, $\mathbf{W}$ a data weighting matrix, and $\mathbf{R}$ a (real-valued) matrix evaluating the (first-order) spatial roughness of $\mathbf{m}$. Under the assumption that the data errors are uncorrelated and normally distributed, $\mathbf{W}$ is a diagonal matrix, with its entries in this study being estimated from the analysis of impedance data pairs measured in normal and reciprocal configurations (Koestel et al. 2008; Flores Orozco et al. 2012b). At each iteration step, a univariate search is performed to find the optimum value of the regularization parameter λ which locally minimizes the data misfit. The model update, $\Delta\mathbf{m}$, is calculated from solving the linear system of equations

$$\left[\mathbf{J}^{\mathrm{H}}\mathbf{W}^{\mathrm{H}}\mathbf{W}\mathbf{J} + \lambda\mathbf{R}^{\mathrm{T}}\mathbf{R}\right]\Delta\mathbf{m} = \mathbf{J}^{\mathrm{H}}\mathbf{W}^{\mathrm{H}}\mathbf{W}\left[\mathbf{d} - \mathbf{f}(\mathbf{m})\right] - \lambda\mathbf{R}^{\mathrm{T}}\mathbf{R}\mathbf{m}, \tag{1.2}$$

where $\mathbf{J}$ is the Jacobian matrix computed for the given model $\mathbf{m}$, H denotes the Hermitian (complex conjugate transpose), and T the transpose matrix. The iteration process is stopped when the root-mean-square data-misfit value reaches the value of 1 for a maximum possible λ, yielding the smoothest spatial distribution explaining the data.

1.2.2 EIT Inversion with Spatio-Spectral Regularization

Current complex conductivity (or complex resistivity) imaging approaches are limited to the inversion of single-frequency data (e.g., Kemna et al. 2004; Blaschek et al. 2008), or the independent inversion of multi-frequency data sets (e.g., Kemna et al. 2000; Flores Orozco et al. 2012a, 2013). Such an approach limits the characterization capabilities of EIT because there is no control on the spectral behavior in the inversion procedure, resulting in considerable ill-posedness with respect to the retrieval of spectral characteristics. In order to overcome this deficiency, we implemented an extended EIT inversion scheme with full spatio-spectral regularization for the simultaneous inversion of multi-frequency impedance data sets by adding an additional smoothness constraint with respect to the spectral dimension.

Let $\mathbf{m}_f$, $\mathbf{d}_f$, $\mathbf{J}_f$, and $\mathbf{W}_f$ denote the extended model vector, the data vector, the Jacobian matrix, and the data weighting matrix, respectively, that contain all model vectors $\mathbf{m}_i$, data vectors $\mathbf{d}_i$, Jacobian matrices $\mathbf{J}_i$, and data weighting matrices $\mathbf{W}_i$ for N measurement frequencies ($i = 1, \ldots, N$):

$$\mathbf{m}_f = \begin{pmatrix} \mathbf{m}_1 \\ \vdots \\ \mathbf{m}_N \end{pmatrix}, \; \mathbf{d}_f = \begin{pmatrix} \mathbf{d}_1 \\ \vdots \\ \mathbf{d}_N \end{pmatrix}, \; \mathbf{J}_f = \begin{pmatrix} \mathbf{J}_1 & & \\ & \ddots & \\ & & \mathbf{J}_N \end{pmatrix}, \; \mathbf{W}_f = \begin{pmatrix} \mathbf{W}_1 & & \\ & \ddots & \\ & & \mathbf{W}_N \end{pmatrix}. \tag{1.3}$$

Note that $\mathbf{J}_f$ and $\mathbf{W}_f$ are block diagonal matrices. For simultaneously inverting the data $\mathbf{d}_f$ we solve the extended linear system of equations

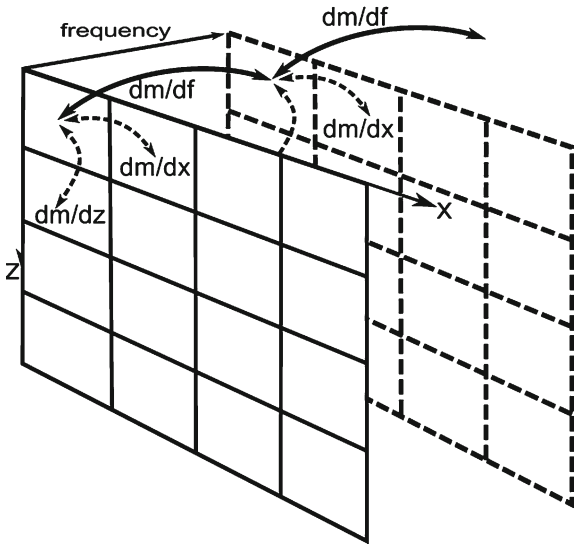

Fig. 1.1 Spatio-spectral regularization scheme implemented in the multi-frequency EIT inversion. The indicated planes represent the spatial model parameterization (lumped finite-element cells in the *x*,*z*-plane) at two successive frequencies (*f*). In addition to its adjacent neighbors in space, each model parameter is coupled to its adjacent "spectral" neighbor (same location in space, but for next frequency)

$$\left[\mathbf{J}_f^{\mathrm{H}}\mathbf{W}_f^{\mathrm{H}}\mathbf{W}_f\mathbf{J}_f + \lambda\mathbf{R}_f^{\mathrm{T}}\mathbf{R}_f\right]\Delta\mathbf{m}_f = \mathbf{J}_f^{\mathrm{H}}\mathbf{W}_f^{\mathrm{H}}\mathbf{W}_f\left[\mathbf{d}_f - \mathbf{f}_f(\mathbf{m}_f)\right] - \lambda\mathbf{R}_f^{\mathrm{T}}\mathbf{R}_f\mathbf{m}_f, \tag{1.4}$$

with correspondingly extended forward model response $\mathbf{f}_f$ and model update $\Delta\mathbf{m}_f$, where spatio-spectral smoothing is realized by an extended model roughness matrix, $\mathbf{R}_f$, given by

$$\mathbf{R}_f = \begin{pmatrix} \mathbf{R}_1 & 0 & \cdots & 0 \\ 0 & \mathbf{R}_2 & \ddots & \vdots \\ \vdots & \ddots & \ddots & 0 \\ 0 & \cdots & 0 & \mathbf{R}_N \end{pmatrix} + \lambda_f \begin{pmatrix} -1 & 0 & \cdots & 0 & 1 & 0 & \cdots & 0 \\ 0 & \ddots & \ddots & \vdots & \ddots & \ddots & \ddots & \vdots \\ \vdots & \ddots & -1 & 0 & \cdots & 0 & 1 & 0 \\ 0 & \cdots & 0 & -1 & \ddots & \vdots & \ddots & 1 \end{pmatrix}. \tag{1.5}$$

In Eq. (1.5), $\mathbf{R}_i$ denote the spatial roughness matrices (generally identical for all measurement frequencies), and the second matrix on the right-hand side contains non-zero entries only at the diagonal element and at one off-diagonal element that correspond to the model parameters at the same location in space but for two successive frequencies (Fig. 1.1). Here, the values –1 and 1 are only indicative; actually the true spectral gradient of the model with respect to log frequency is implemented. The spectral regularization strength in the inversion can be adjusted with the additional regularization parameter λ_f.

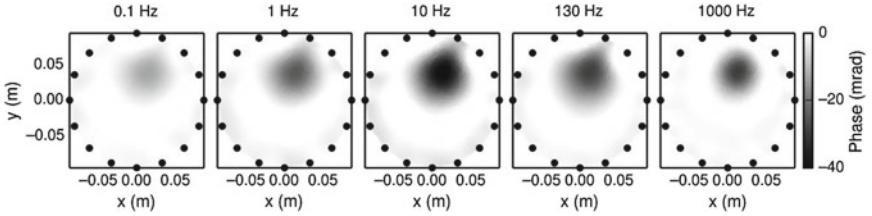

Fig. 1.2 EIT phase images of a cylindrical copper target in a water-filled cylindrical tank at five selected measurement frequencies computed with spatio-spectral regularization. *Black dots* indicate position of electrodes used for data acquisition

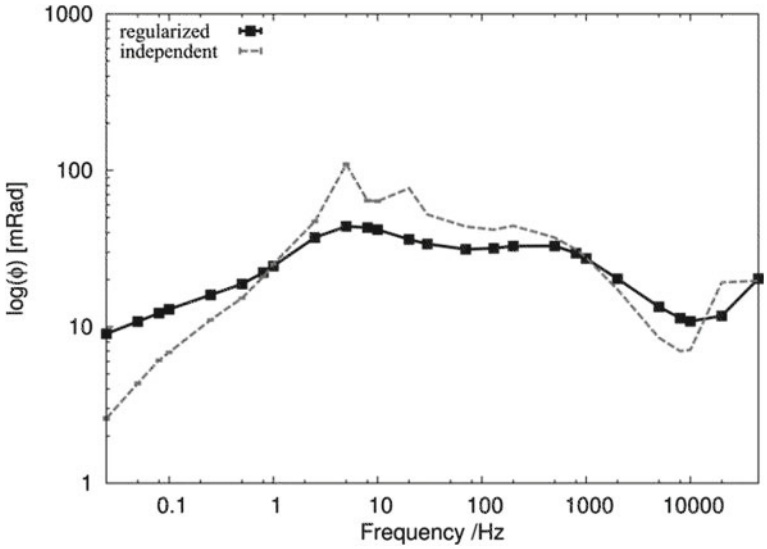

Fig. 1.3 Recovered phase spectrum at the center of the copper target (cf. Fig. 1.2) using independent single-frequency inversions (*dashed grey curve*) and the new multi-frequency inversion with spectral regularization (*solid black curve*)

1.2.3 Validation Using a Physical Tank Model

In order to compare single-frequency inversions with inversion results obtained with additional spectral regularization, EIT measurements were made on a copper cylinder positioned within a water-filled cylindrical tank using the laboratory EIT system described in Zimmermann et al. (2008b). The copper target can easily be identified by the high phase values in the reconstructed images (Fig. 1.2). The phase spectrum extracted from the EIT images at the center of the copper target reveals rather erratic spectral variations, especially in the frequency range between 1 and 100 Hz, where highest polarization is observed for the single-frequency inversions (Fig. 1.3). This reflects the inherent ill-posedness of a non-spectrally regularized inversion approach

with respect to the recovery of spectral variations. With the new spatio-spectral regularization approach, the inverted spectral phase values show a more consistent, smoothly varying behavior, in agreement with the typical dispersion characteristics of electrical relaxation processes. It is clear that the choice of the regularization parameter λ_f in Eq. 1.5 controls the amount of spectral smoothing, and future studies will need to establish methods to determine the most appropriate values of λ_f.

1.3 Inductive and Capacitive Coupling Effects: Modeling and EIT Data Correction

1.3.1 Design of EIT Field System and Borehole Electrode Chains

In order to image the spectral phase response of low-polarizable soils and rocks, spectral EIT measurements with high phase accuracy in a broad frequency range are needed. It is challenging to design EIT data acquisition to achieve such a high accuracy, especially in the high frequency range (100 Hz to 45 kHz). Previous work focused on the development of a laboratory spectral-EIT measurement system with sufficient accuracy (Zimmermann et al. 2008b). On the basis of this laboratory system, a prototype for spectral EIT data acquisition at the field scale was realized (Zimmermann et al. 2010; Zimmermann 2011). Both systems have a modular design with active electrode modules consisting of integrated amplifiers for electric potential measurements and integrated switches for current injection. To achieve the required high accuracy, the developed EIT systems rely on model-based correction methods to minimize the remaining errors of the system. The errors that have been corrected in such a manner are related to amplification, signal drift, and propagation delay of the signal due to the long cables, amongst other error sources.

For borehole EIT measurements, electrode chains and logging tools have recently been developed and constructed. The borehole chains consist of eight active electrode modules with an electrode spacing of 100 cm, whereas the borehole logging tool consists of four electrode modules with an electrode spacing of 16.2 cm. For the electrical connection of the active electrode modules to the EIT data acquisition system, a 25 m long shielded multicore cable is used in both cases (Zhao et al. 2013).

1.3.2 Electromagnetic Coupling

The necessary use of long cables in the design of borehole electrode chains introduces additional errors in the phase measurements due to electromagnetic coupling effects; these effects can be separated in (i) inductive coupling between the long electric loops for current injection and potential measurement, and (ii) capacitive coupling between the cable and the electrically conductive environment. Both types

of coupling currently limit the upper frequency for accurate EIT measurements to the tens of Hz range. The phase errors due to electromagnetically induced eddy currents in the subsurface are small in relation to these two effects and can be neglected for the application considered here.

The inductive coupling using two borehole chains can be divided into two cases: (i) coupling within one electrode chain and (ii) coupling between two different electrode chains. In the first case, the electrical wires in a single multicore cable are close together and this leads to strong inductive coupling. It is important to note that the strength of this coupling depends only on the design of the multicore cable and not on the cable layout during field measurements. In the second case, the coupling is weaker due to the larger separation between the electrical wires. However, the strength of the coupling depends on the position of the multicore cable layout during field measurements, which must therefore be determined or controlled in order to allow adequate corrections for inductive coupling. However, the cable separations only need to be known with cm accuracy. In summary, a configuration with current injection and voltage measurement in one borehole belongs to the first case, and a configuration with current injection in one borehole and voltage measurement in a second borehole belongs to the second case. All other configurations can be obtained by superpositioning of these two types.

Here, we present correction methods for inductive coupling in one multicore cable and capacitive coupling between the borehole chains and the subsurface. The correction of inductive coupling in one cable is a complicated task because the separation between the wires needs to be known with an accuracy better than 0.1 mm. In addition, the inductive coupling is also influenced by eddy currents in the outer shielding of the chain.

1.3.3 Correction Methodology

Inductive coupling leads to a parasitic additive imaginary part in the measured transfer impedances. Typically, a wide range of four-electrode configurations is used to measure the electrical impedance of the subsurface. This electrical transfer impedance Z_M is the ratio of the measured voltage U_M between two potential electrodes and the injected current I_I between two excitation electrodes. Each electrode is connected with one wire which is parallel to the other wires in the case of current injection and voltage measurement in one borehole (Fig. 1.4). The active elements in the electrode modules can be neglected for the consideration of the inductive effects.

Due to the inductive coupling between the two wire pairs, an additional voltage U_{II} in loop II is induced from the injected current I_I in loop I (Fig. 1.4). This means that the injected current leads to an impedance Z_S of the subsurface and the unwanted induced impedance Z_{IC}. This results in the total measured transfer impedance

$$Z_M = Z_S + Z_{IC} = Z_S + j\omega M. \tag{1.6}$$

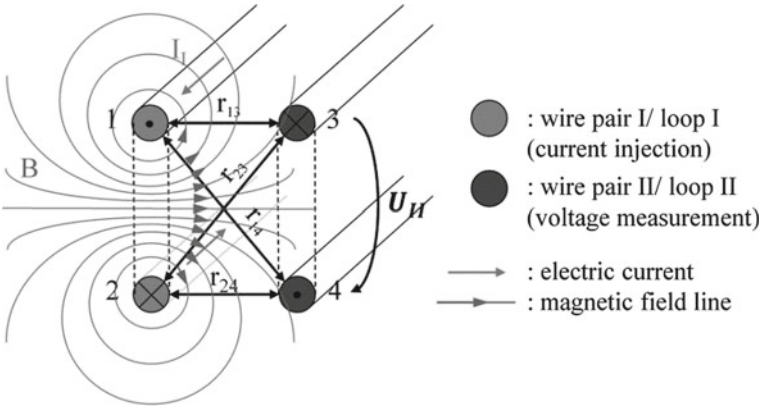

Fig. 1.4 Mutual induction between two parallel electrical wire pairs (from Zhao et al. 2013)

This equation shows that the error due to inductive coupling can be removed by subtracting the coupling impedance Z_{IC}, which is the mutual inductance M multiplied by the imaginary unit j and the angular frequency ω, from the measured transfer impedance.

In order to determine the exact coupling impedances, we have evaluated several approaches. In a first approach, we tried to determine the values based on the geometry of the multicore cable. However, it is not possible to determine the wire positions within the multicore cable with the required accuracy. In addition, eddy currents in the electrical shield have a big influence on the impedance in the kHz frequency range. Therefore, this approach was abandoned. In an alternative approach, we measured the mutual inductance for all possible electrode configurations (Zhao et al. 2013). This is cumbersome and time-consuming for practical use. To overcome this practical problem, the latest calibration method relies on a pole-pole matrix

$$\mathbf{P} = \begin{bmatrix} \mathbf{A} & \mathbf{B} \\ \mathbf{C} & \mathbf{D} \end{bmatrix}, \tag{1.7}$$

with coupling impedances derived from pole-pole calibration measurements. The matrix **A** contains the coupling impedances between the wires of the first borehole chain, and the matrix **D** contains the coupling impedances between the wires of the second borehole chain. The matrices **B** and **C** contain the coupling impedances between the wires of different borehole chains. The strength of these couplings depends on the position of the multicore cable layout during field measurements and can be calculated using equations provided in Sunde (1968). This calculation is not treated here. In the future, we will also consider this case of coupling.

In order to obtain the coupling impedances in one borehole chain (matrices **A** and **D**) using pole-pole (i.e., ground-based) current injection and voltage measurements, all electrodes of the chain are short-circuited and connected to the ground of the